European Conference on Computational Fluid Dynamics
ECCOMAS CFD 2006
P. Wesseling, E. Oñate, J. Périaux (Eds)

NUMERICAL STUDY OF TURBULENT FLOW AROUND A SQUARE CYLINDER USING TWO LOW-REYNOLDS-NUMBER $k-\varepsilon$ MODELS

Mehrdad Raisee* and Azadeh Jafari†

* Department of Mechanical Engineering, Faculty of Engineering,
University of Tehran, Tehran, Iran
e-mail: mraisee@ut.ac.ir

† Department of Mechanical Engineering, Faculty of Engineering,
University of Tehran, Tehran, Iran
e-mail: a_jafari@me.ut.ac.ir

Keywords: Vortex Shedding, Square Cylinder, Turbulence Modeling, Eddy Viscosity Model

Abstract. *This paper discusses the abilities of two different low-Reynolds-number $k-\varepsilon$ eddy-viscosity models in resolving the complex physical features that arises in turbulent flows around a square cylinder at Re=22000. For the modeling of turbulence, the Launder & Sharma (LS) [1] and Kawamura & Kawashima (KK) [2] low-Re $k-\varepsilon$ models have been employed. The present numerical results were obtained using a two-dimensional finite-volume code. The pressure field is obtained with the well-known SIMPLE algorithm. Advective volume-face fluxes are approximated using a bounded version of the upstream quadratic interpolation scheme, QUICK. Comparisons of the numerical results with the experimental data indicate that the steady computations, as expected, cannot produce reliable flow field predictions in the wake region downstream of the square cylinder. Consequently, the time derivatives of dependent variables are included in the transport equations and are approximated using the second-order Crank-Nicholson scheme. The unsteady computations significantly improve the predictions and the results of unsteady simulations with both turbulence models are in closer agreement with measurements compare to the steady predictions. The predicted value for St number is 0.126 and 0.123 using the LS and KK turbulence models respectively which are in good agreement with the measured value of 0.132. The unsteady predictions using the LS model are in better agreement with the measured data than those obtained with the KK model. Both turbulence models fail to produce reliable turbulence field predictions and, thus, it is necessary to apply more advance turbulence models, such differential stress models, for more accurate predictions of such flows.*

NOMENCLATURE

A= Cross section area

C_D = Drag Coefficient ($C_D = \dfrac{\int_A PdA}{1/2\rho A U_{in}^2}$)

D= Cylinder dimension

f = Shedding frequency

H= Channel height
k = Turbulent kinetic energy
P = Pressure
P_k = Production term
Re= Reynolds number ($\mathrm{Re} = U_{in} D / \nu$)
St = Strouhal number ($St = \frac{fD}{U_{in}}$)
t= time
U_i = Mean velocity components(U,V)
$\overline{u_i u_j}$ = Reynolds stress tensor
x_i = Cartesian coordinate (x,y)

Greek letters
β = Aspect ratio (β =D/H)
ε = Dissipation rate
$\tilde{\varepsilon}$ = Isotropic dissipation rate
δ_{ij} = Kronecker delta
τ = Period of time
μ = Dynamic viscosity
ν = Kinematic viscosity
ρ = Density

1 INTRODUCTION

Turbulent flow around bluff bodies has been attracted increasing attention not only because of its academic attractiveness but also due to its relevant practical concerns associated with energy conservation and structural design. For instance, fuel consumption of aircraft and road vehicles may be decreased by reducing the aerodynamic drag and multi-story buildings such as sky-scrapers can be designed in a way to avoid potentially disastrous wind-induced oscillations. One of the basic geometry in bluff body configurations is flow over a square cylinder confined in a channel or subjected to a free-stream flow. In such flow, various complex physical phenomena including flow separation, reattachment, recirculation, and vortex shedding occurs, producing a very challenging flow field for both experimentalist and also CFD practitioners.

Over the last two decades, a vast amount of experimental and numerical studies has been conducted to increase the understanding of different physical processes of flow past a square cylinder. Lee [3] presented mean and fluctuating pressure fields for flow around a square cylinder in both uniform and turbulent flows. He observed that the rotation of the cylinder with respect to the flow moves the vortex region downstream and as a result of that the drag force decreases. Bearman and Trueman [4] studied turbulent flow around a rectangular cylinder at a range of Reynolds number from $\mathrm{Re}=2\times10^4$ to 7×10^4. Detailed measurements for pressure field, mean drag force and shedding frequency as well as flow visualization were presented. One of the most extensive investigations was carried out by Okajima [5]. He

determined Strouhal number of flow around a rectangular cylinder with aspect ratios of 1 to 4 in a range of Reynolds number between 2×10^4 to 7×10^4. For aspect ratios of 2 and 3, he found a certain range of critical Reynolds number in which abrupt flow patterns cause sudden discontinuity in Strouhal number. Knisely [6] experimentally determined Strouhal numbers for a family of rectangular cylinders with aspect ratio of ranging from 0.04 to 1 with angel of attack 0^{o} to 90^{o}. Measurements were conducted both in water channel in Reynolds numbers between 7.2×10^2 and 3.1×10^4 and in a wind tunnel with Reynolds numbers between 8.8×10^3 and 8.1×10^4. He found that the Strouhal numbers, except for the thinnest plate, have qualitatively similar behavior with changing angel of attack. The general tendency is a rapid rise in the Strouhal number occurs at relatively small angle of attack. This rapid rise associated with reattachment of the separate shear layer. Norberg [7] studied fluid flow around rectangular cylinders and measured pressure forces at the angles of attack 0^{o} to 90^{o}. In this investigation the aspect ratios of the obstacle were 1 to 5 and Reynolds number ranged from 400 to 3×10^4. The results of this investigation showed a large influence of both angle of attack and aspect ratio on the flow structure due to reattachment and shear layer/edge interactions. Lyn and Rodi [8] and Lyn et al. [9], using LDV, measured velocity components and Reynolds stresses for turbulent flow around a square cylinder at Re=21400. Phase (ensemble) averaged velocity and turbulence intensities were presented in various locations along the top surface of the obstacle and within the wake region downstream of the obstacle. They found a close relationship in phase amplitude between phase-average intensities and gradient of phase average velocity.

An early computer simulation of unsteady flow around an obstacle at low Reynolds numbers was reported by Fromm and Harlow [10]. They studied the development of a vortex street behind a plate which has impulsively accelerated to constant speed in a channel of finite width. In their study, the Reynolds number ranged between 15 and 6000. However, only a few results appeared in their paper. Davis et al. [11] numerically investigated the effects of channel walls on the flow around a square cylinder. They concluded that the presence of walls can leads to significant changes in the flow characteristics and increases both the drag coefficient and Strouhal number. Tamura and Kuwahara [12] investigated the aerodynamics behavior of flow around a cylinder placed in a uniform stream at high Reynolds numbers. They obtained the numerical solutions for unsteady flow for various 2-D and 3-D test cases by formulating the 2-D and 3-D incompressible Navier-Stocks equations in a generalized coordinate system. No turbulence models were employed in their computations and the convective terms in Naveir-Stocks equations were approximated using the third order upwind scheme. They found that the flow patterns obtain by 2-D Navier-Stocks equations have significant differences from that return by the 3-D. Moreover, the computational results revealed that 3-D structures decrease both the drag coefficient and the lift amplitude. Hence, the authors concluded that the 3-D computational results are closer to the experimental value, than the 2-D results. Kawamura and Kawashima [2] using a low Reynolds $k-\tilde{\varepsilon}$ model examined unsteady turbulent flow around a square confined in channel. They compared their numerical results at Re=22000 with the experimental data of Lyn et al. [9]. The calculated turbulence levels behind the cylinder was significantly lower than the experimental data.

However, the predicted practical quantities (Strouhal number and drag coefficient) and also the averaged velocity profiles were in satisfactory agreement with the measured data.

The present work focuses on the prediction of the steady and unsteady two-dimensional turbulence flow over a square cylinder, see Figure 1. The main objective of the present study is to investigate the effectiveness of two different low-Reynolds number $k-\varepsilon$ models in predicting turbulent flow characteristics over a square cylinder.

2 PROBLEM DESCRIPTION AND BOUNDARY CONDITIONS

Figure 1 shows the geometry of two-dimensional square cylinder investigated in this study. The computational domain consists of a square cylinder of length-side D and of blockage ratio ($\beta = \mathrm{D}/\mathrm{H}$) of 0.07 which is located in the center of the channel. The channel height is chosen as H=14D to remove the effects of channel walls on the flow field. The distance of the obstacle center from the inlet and outlet of the channel are 4.5D and 14.D respectively. The channel is wide enough along the span-wise direction, thus, the 3-dimensional effects of side walls are ignored. The Reynolds number based on inlet velocity and D is 22000.

No-slip boundary conditions are used at the all walls. In accordance with the experiment of Lyn et al. [9], a uniform flow is assumed for the inlet of the channel. The inlet turbulent energy is set to $k_{in} = (0.02U_{in})^2$. The dissipation is set to $\varepsilon_{\mathrm{in}} = k_{in}^{3/2}/L$ with $L = 0.2D$. At the outlet boundary, a zero gradient boundary condition is used for k and ε. For U, a convective type boundary condition of form:

$$\frac{\partial U}{\partial t} + U_{in}\frac{\partial U}{\partial x} = 0 \tag{1}$$

is used, while the cross-stream component (V)is set to zero.

3 GOVERNING EQUATIONS

For an unsteady, Newtonian, incompressible flow, the conservation of laws of mass and momentum obtained with the ensemble averaging are written as:
Continuity:

$$\frac{\partial U_j}{\partial x_j} = 0 \tag{2}$$

Momentum:

$$\frac{\partial U_i}{\partial t} + \frac{\partial (U_i U_j)}{\partial x_j} = -\frac{1}{\rho}\frac{\partial P}{\partial x_i} + \frac{\partial}{\partial x_j}\left(\nu\frac{\partial U_i}{\partial x_j} - \overline{u_i u_j}\right) \tag{3}$$

where P is the pressure, U_i denotes mean velocities and $\overline{u_i u_j}$ are the unknown Reynolds stresses.

4 TURBULENCE MODELING

In this study the Launder and Sharma [1] and Kawamura and Kawashima [2] low-Reynolds-number $k-\varepsilon$ models are used for modeling of turbulence. In both EVMs, the Reynolds stresses are obtained via Boussinesq hypothesis [13], shown blow:

$$\overline{u_i u_j} = \frac{2}{3}k\delta_{ij} - \nu_t\left(\frac{\partial U_i}{\partial x_j} + \frac{\partial U_j}{\partial x_i}\right) \tag{4}$$

where ν_t is obtained by solving transport equations for turbulent kinetic energy (k) and its dissipation rate (ε)

4.1 Launder and Sharma low-Re $k-\varepsilon$ model (LS)

This model is an extension of high-Re $k-\varepsilon$ model that accounts for the wall damping of turbulence and hence can be used across the viscous sub-layer. The turbulent viscosity is obtained from equation (5):

$$\nu_t = c_\mu f_\mu \frac{k^2}{\tilde{\varepsilon}} \tag{5}$$

where c_μ coefficient is given in Table 1.

The distributions of k and ε, are obtained by solving transport equations for these quantities. These transport equations are written as:

$$\frac{Dk}{Dt} = \frac{\partial}{\partial x_j}\left[\left(\nu + \frac{\nu_t}{\sigma_k}\right)\frac{\partial k}{\partial x_j}\right] + P_k - \tilde{\varepsilon} - 2\nu\left(\frac{\partial\sqrt{k}}{\partial x_j}\right)^2 \tag{6}$$

$$\frac{D\tilde{\varepsilon}}{Dt} = \frac{\partial}{\partial x_j}\left[\left(\nu + \frac{\nu_t}{\sigma_\varepsilon}\right)\frac{\partial\tilde{\varepsilon}}{\partial x_j}\right] + f_1 c_{\varepsilon 1}\frac{\tilde{\varepsilon}}{k}P_k - f_2 c_{\varepsilon 2}\frac{\tilde{\varepsilon}^2}{k} + E + S_\varepsilon \tag{7}$$

where variable $\tilde{\varepsilon}$ is the homogeneous dissipation rate which can be related to the real dissipation rate through:

$$\tilde{\varepsilon} = \varepsilon - 2\nu\left[\frac{\partial\sqrt{k}}{\partial x_j}\right]^2 \tag{8}$$

The turbulent kinetic energy production term, P_k, is given by:

$$P_k = -\overline{u_i u_j}\frac{\partial U_i}{\partial x_j} \tag{9}$$

The damping functions f_1, f_2 and f_μ are determined as below:

$$f_1 = 1, \quad f_2 = 1 - 0.3\exp\left(-\tilde{R}_t^{\,2}\right), \quad f_\mu = \exp\left[-3.4\Big/\left(1 + 0.02\tilde{R}_t\right)^2\right] \tag{10}$$

where, $\tilde{R}_t = k^2/\nu\tilde{\varepsilon}$ is the local turbulent Reynolds number.

The constant parameters in the turbulent kinetic energy and its dissipation rate equations are given in Table 1.

$c_{\varepsilon 1}$	$c_{\varepsilon 2}$	c_{μ}	σ_k	σ_{ε}
1.44	1.92	0.09	1.0	1.3

Table 1: Empirical constants for the $k-\varepsilon$ model.

The E term was first introduced by Jones and Launder [14] and is expressed as:

$$E = 2\nu\nu_t \left(\frac{\partial^2 U_i}{\partial x_j \partial x_i} \right)^2 \tag{11}$$

It is well-known that, in separated flows, the Launder and Sharma version of $\tilde{\varepsilon}$-equation returns excessively high levels of near-wall turbulence. To address this problem, Yap [15] introduced an extra source term into the dissipation rate equation, "Yap", based on the wall distance, y.

$$S_{\varepsilon} = Yap = 0.83 \frac{\tilde{\varepsilon}^2}{k} \max\left[(\ell / \ell_e - 1)(\ell / \ell_e)^2, 0 \right] \tag{12}$$

where, ℓ is the turbulent length-scale $k^{3/2}/\tilde{\varepsilon}$, the equilibrium length-scale $\ell_e = 2.55y$, and y is the distance to the wall

4.2 Kawamura and Kawashima low-Re number $k-\varepsilon$ model (KK)

Kawamura and Kawashima [2] examined the balance of the budged terms in the turbulence energy equation and subsequently revised this by including the pressure diffusion term in order to correctly reproduce the behavior of the near-wall dissipation. The other point of this revision was the inclusion of a new extra term in the $\tilde{\varepsilon}$-equation to generate the correct near-wall behavior of y^2. The empirical function f_{μ}, assumed to be a function of the wall distance y, is proposed as follows:

$$f_{\mu} = 1.0 - \exp\{-y_{\eta}/285 - (y_{\eta}/20)^3\} \tag{13}$$

where $y_{\eta} = y/\eta$ and η is the Kolmogorov Scale defined as $\eta = (\nu^3/\varepsilon)^{1/4}$.

Turbulent energy and dissipation rate equations are defined similar to those in Launder and Sharma $k-\varepsilon$ model:

$$\frac{Dk}{Dt} = \frac{\partial}{\partial x_j}\left[\left(\nu + \frac{\nu_t}{\sigma_k} \right) \frac{\partial k}{\partial x_j} \right] + P_k - (\tilde{\varepsilon} + D) + \pi^* \tag{14}$$

$$\frac{D\tilde{\varepsilon}}{Dt} = \frac{\partial}{\partial x_j}\left[\left(\nu + \frac{\nu_t}{\sigma_{\varepsilon}} \right) \frac{\partial \tilde{\varepsilon}}{\partial x_j} \right] + c_{\varepsilon 1} f_1 \frac{\tilde{\varepsilon}}{k} P_k - c_{\varepsilon 2} f_2 \frac{\tilde{\varepsilon}^2}{k} + E + S_{extra} \tag{15}$$

where $C_{\varepsilon 1}$ and $C_{\varepsilon 2}$ coefficients are the same as those given in Table 1. Turbulent Prandtl numbers, σ_k and σ_{ε}, that were constant in LS model are now a function of y_{η} defined blow:

$$\sigma_\varepsilon = \sigma_k = 1.0 - 0.5\exp\{-(\frac{y_\eta}{20})^2\} \tag{16}$$

The extra source term, π_k^*, in turbulent energy is:

$$\pi_k^* = -\frac{1}{2}\nu\frac{\partial}{\partial x_i}\{\frac{k}{\varepsilon}(\frac{D}{\varepsilon})^2\frac{\partial D}{\partial x_i}\} \tag{17}$$

The sink term in dissipation equation is proposed as:

$$S_{extra} = -\tilde{\varepsilon}D/k \tag{18}$$

The expression for E term is similar to that in LS model and is given as:

$$E = c_{\varepsilon 3}\nu\nu_t\left(\frac{\partial^2 U_i}{\partial x_j \partial x_i}\right)^2 \tag{19}$$

where value of constant $c_{\varepsilon 3}$ coefficient is 0.6.

5 NUMERICAL METHOD

The general form of the governing equations of mean flow and turbulence are written as:

$$\underbrace{\frac{\partial}{\partial t}(\rho\phi)}_{Unsteady} + \underbrace{\frac{\partial}{\partial x}(\rho\phi U) + \frac{\partial}{\partial y}(\rho\phi V)}_{Convection} = \underbrace{\frac{\partial}{\partial x}\left(\Gamma_\phi\frac{\partial\phi}{\partial x}\right) + \frac{\partial}{\partial y}\left(\Gamma_\phi\frac{\partial\phi}{\partial y}\right)}_{Diffusion} + \underbrace{S_\phi}_{Source} \tag{20}$$

where x and y are the coordinates in the stream-wise and cross-stream directions respectively and ϕ represents velocity component (U and V) and turbulence quantities (k and ε). Γ_ϕ is an effective diffusion coefficient and S_ϕ denotes the total source term in each transport equation.

In the present study the governing equations are solved using finite-volume methodology in a semi-staggered grid system. In such a grid distribution, both velocity components are computed and stored in the same nodal position and the velocity nodes are located at the corners of the scalar control volume. Thus, only two sets of control volume is needed for the computations. The pressure field is linked to that of velocity through the well-known SIMPLE pressure correction algorithm. To avoid stability problems associated with pressure-velocity decoupling the Rhie and Chow [16] interpolation scheme is also employed. The third order QUICK differencing scheme is employed for approximation of the convective terms in all transport equations. In QUICK scheme, depending on the flow direction, the value of unknown dependent variable ϕ at each face of control volume is evaluated from a quadratic polynomial which passes through a grid point downstream and two grid points upstream of each face. For example, as shown in Figure 2, the value of ϕ at the east face of control volume ϕ on a uniform grid is obtained by:

$$\phi_e = \begin{cases} \phi_P + Q_e^+ & F_e > 0 \\ \phi_E + Q_e^- & F_e < 0 \end{cases} \tag{21}$$

where ϕ_p and ϕ_E are the values of upwind approximation and QUICK scheme corrections Q_e^+ and Q_e^- are:

$$Q_e^+ = \frac{1}{8}\left[-\phi_W + 3\phi_E - 2\phi_P\right] \tag{22}$$

$$Q_e^- = \frac{1}{8}\left[-\phi_{EE} + 3\phi_P - 2\phi_E\right] \tag{23}$$

In the unsteady calculations the time derivatives are approximated using the second-order Crank-Nicholson [17]. Obviously, the time step in the time-marching calculation of vortex shedding flow is an important parameter. If a very large value is chosen, the global accuracy may be seriously affected. By considering both the accuracy and computational time, a non-dimensional time step of $\Delta t = 6\times10^{-9}$ is used. This time step, which is proportional to H/U_{in}, is found to give fairly accurate results.

As shown in Figure 3, the grid used for computations consist of 105×102 grid nodes in the stream-wise (x) and cross-stream (y) directions respectively. For this grid, the y^+ values of the near-wall nodes are less than unity.

6 RESULTS AND DISSCUTION

In this section the abilities of low-Re number $k-\varepsilon$ models (described in Section 4) in reproducing flow characteristics are investigated.

In order to show how steady solution of governing equations results in unphysical predictions, the predicted velocity vectors using the steady simulation and low-Re $k-\varepsilon$ Launder and Sharma model are shown in Figure 4. To show the details of flow field in the wake region, the velocity vectors are magnified in this region. The steady simulation shows that the flow separates at the leading edges of the cylinder forming two intense recirculation bubbles near the lower and upper surfaces of the obstacle. Moreover, a pair of large, symmetric contour rotating vortices are formed downstream of the obstacle. These predictions are in contradictions with experimental results of [7] and [8] which indicate asymmetric flow behavior in the wake region downstream of the obstacle.

Instantaneous streamlines ($-10000<\psi<10000$) obtained with the unsteady simulation and LS model, during one period of vortex shedding, are demonstrated in Figure 5. As can be noted, there is a vortex in development at the lower base corner at $t/\tau = 3/20$, being fed by the separation and recirculation at the lower face of the obstacle. As it grows, the attachment point on the rear side is being pushed downward. When the attachment point reaches the upper base corner at $t/\tau = 13/20$, a new vortex is about to be formed at that corner. As this new vortex grows, the old vortex is being pushed away and is eventually shed to the wake. In general, the same trend occurs in the other periods.

From practical point of view, two of the most important parameters for unsteady flow around a cylinder are Strouhal number and drag coefficient. The predicted values for these parameters, using turbulence models used in this work, are compared with experimental data of Lyn et al. [8] in Table 2. While the values predicted with both models are close to the measured values, the predicted values of Strouhal number and drag coefficient using LS

model are more accurate.

	St	C_D
Exp. (Lyn et al [8])	0.132	2.1
KK model	0.123	1.90
LS model	0.126	1.98

Table 2: Strouhal number and Drag coefficient.

Figure 6 shows distribution of time-averaged U-velocity along the channel centerline. While the steady predictions for U with both turbulence models are much lower than measured data, the unsteady predictions are in close agreement with experimental data. In the wake region, the unsteady prediction of U with the LS model is generally in better agreement with the experimental data.

The steady and unsteady predictions of U-velocity with both turbulence models at several location are compared with the experimental data in Figure 7. Over the obstacle at $x/D = -0.5$, 0.0 and 0.5, the steady and unsteady predictions of stream-wise velocity profiles with both turbulence models are in good agreement with experimental data. Note that, at the first section within wake, i.e. at $x/D = 1.0$, the most accurate profile returns using unsteady solution and LS model. Further downstream at $x/D = 1.5 \text{ to } 8.0$, there are significant differences in predicted U-velocity profiles with steady and unsteady solution and also with the LS and KK turbulence models. As can be seen in this figure, unsteady solution of transport equations significantly improves the predictions. Moreover, the unsteady simulation with the LS model produces more accurate stream-wise velocity predictions than the KK model.

The steady and unsteady predictions of cross-stream velocity with two turbulence models are compared with the experimental data in Figure 8. At the first station, i.e. $x/D = -0.5$, there is a good agreement between numerical results with the measured data. At the second station, i.e. $x/D = 0$, there is significant difference between the steady and the unsteady predictions with both turbulence models and as can be noted the unsteady solutions produce more accurate profiles for V-velocity. Furthermore, the unsteady results using the LS model are in the better agreement with the experimental data. At the first station within the wake, i.e. $x/D = 1.0$, the results of unsteady computations, especially those obtained with the LS model, are in better agreement with the experimental data. The steady predictions with both turbulence models predict almost zero values for V-velocity which do not confirm with experiment. At $x/D = 2.0$, the differences between the LS and KK models in unsteady solutions are less. The superior performance of the LS model compare to the KK model and the more accurate predictions of unsteady solution compare to the steady solution are clearly observed at $x/D = 2.5$. As can be noted, at the further downstream, the differences between the steady and unsteady, compare to upstream stations, are less. This is expected, since at the stations far a way from the cylinder the flow is essentially steady. Thus, the steady and unsteady simulations return similar results.

Attention is now directed towards the prediction of turbulence field. The predicted stream-wise (u') and cross stream-wise (v') velocity fluctuations using the steady and unsteady simulations are compared with measurements in Figures 9 and 10 respectively. It is clear that both turbulence models seriously underpredicted the experimental data. These figures also revel that the distribution of turbulent intensity profiles are better reproduced with the unsteady simulation. The underprediction of turbulence levels may be due to the fact that both turbulence models used in this study are essentially isotropic and thus are not able to reproduce the turbulence field correctly.

7 CONCLISION

In this paper two low-Reynolds-number $k-\varepsilon$ models have been employed to investigate turbulence flow around a square cylinder. Based on the results presented in this paper it can be concluded that the steady solution of governing equations cannot produce accurate flow predictions and it is necessary to perform unsteady calculations for reliable predictions of such flows. It was found that the Launder and Sharma low-Re $k-\varepsilon$ model reproduces the flow characteristic more accurately than the Kawamura and Kawashima low-Re $k-\varepsilon$ model and as a result of that predicts more accurate values for Strouhal number and drag coefficient. However, both turbulence models fail to produce correct levels for turbulence intensities. Therefore, it is necessary to apply more advance turbulence models such as non-linear eddy viscosity models or differential stress models for accurate predictions of such flows.

AKNOWLEGHMENT

The authors would like to thank the University of Tehran for providing financial support for this study.

REFERENCES

[1] B.E. Launder and B.L. Sharma, *Application of the Energy Dissipation Model of Turbulence to the Calculation of Flow Near a Spinning Disc*, Letter in Heat Mass Transfer, Vol. 1, 131-138 (1974).

[2] H. Kawamura and N. Kawashima, *An Application of a Near-Wall $k-\tilde{\varepsilon}$ Model to the Turbulent Channel Flow with Transpiration and to the Oscillatory Flow around a Square Cylinder*, 2nd Int. Symposium on Turbulence, Heat and Mass Transfer, 379-388 (1997).

[3] B.E. Lee, *The Effect of Turbulence on the Surface Pressure Field of a Square Prism*, J. Fluid Mech., 69, 263-282 (1975).

[4] P.W. Bearman and D.M. Trueman, *An Investigation of the Flow around Rectangular Cylinder,* Aeronautical Quarterly, 23, 229-237 (1972).

[5] A. Okajima, T. Nagashisa and A. Rokugoh, *A Numerical Analysis of Flow around Rectangular Cilindres*, JSME Int. J. ser. II, 33, 702-711 (1990).

[6] C.W. Knisely, *Strouhal Number of Rectangular Cylinder at Incidence: A Review and New Data*, J. of Fluids and Structures, 4, 371-393 (1990).

[7] C. Norberg, *Flow around Rectangular Cylinders: Pressure Forces and Wake Frequencies*, J. Wind, Eng. Ind. Aero., 49, 187-196 (1993).

[8] D.A. Lyn. and W.Rodi, *The Flapping Shear Layer Formed by Flow Separation from the Forward Corner of a Square Cylinder,* J. of Fluid Mechanics, 267, 353-376 (1994).
[9] D.A. Lyn, S. Einva, W. Rodi and J.H. Park, *A Laser-Doppler Velocimetry Study of Ensemble Averaged Characteristics of the Turbulent Near Wake of a Square Cylinder,* J. of Fluid Mechanical, 304. 285-319 (1995).
[10] J.E. Fromm and F.H. Harlow, *Numerical Solution of the Problem of Vortex Street Development,* Physic of Fluid, 6, 975-982 (1963).
[11] R.W. Davis, E.F. Moor and L.P.Purtell, *A Numerical Experimental Study of Confined Flow around Rectangular Cylinders,* Phys. Fluids, 27, 40-59 (1984).
[12] T. Tamura, E. Krause, S. Shirayama, K. Ishii and K. Kuwahara, *Tree Dimensional Computation of Unsteady Flows around a Square Cylinder,* 11th International Conference on Numerical Method in Fluid Dynamics, Williamsburg (1988).
[13] J. Boussinesq, *Theories de Lecoulment Tourbillant,* Mem. Pres. Par Div. Savant a Local Sci. Paris, 23-46(1877).
[14] W.P. Jones and B.E. *Launder, The Prediction of Laminarization with a Two Equation Model of Turbulence,* Int. J. Heat & Mass Transfer, 15, 301-314 (1972).
[15] C.R. Yap, *Turbulent Heat Transfer and Momentum Transfer in Reticulating and Impinging Flow*, PhD. Thesis, Faculty of Technology, University of Manchester, UK (1987).
[16] C.M. Rhie and W.L. Chow, *Numerical Study of the Turbulent Flow Past an Airfoil with Trailing Edge Separation,* AIAA J., 21, 1525-532 (1983).
[17] J. Crank and P. Nicholson., *A Practical Method for Numerical Evaluation of Solutions for Partial Differential Equations of the Heat Conduction*, Proc. Camb. Phill. Soc., 43, 50-67 (1974).

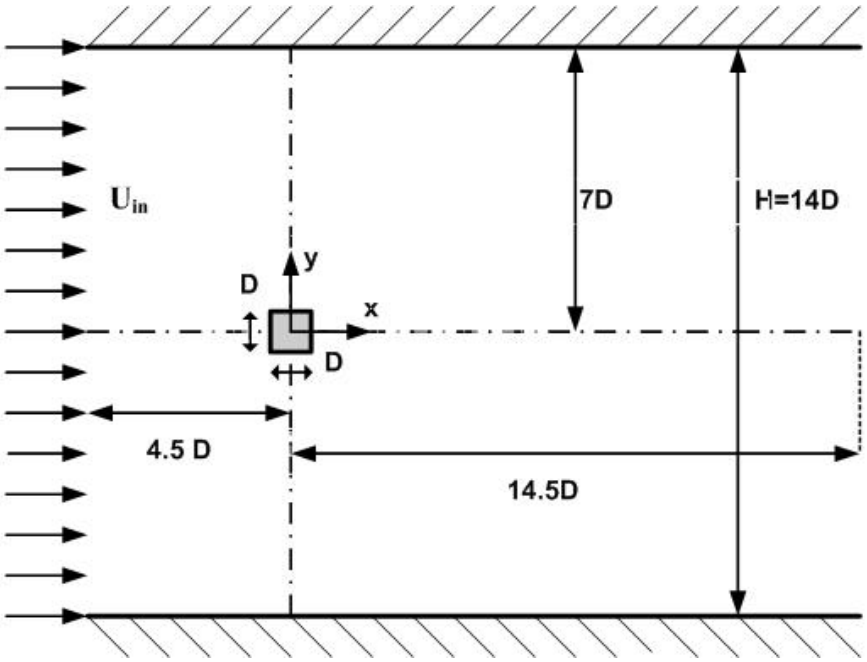

Figure 1: Flow configuration investigated (β = 7% Re=22000).

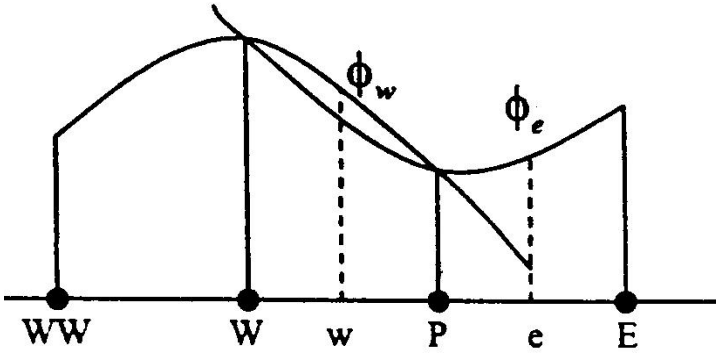

a) $F_e > 0$ and $F_w > 0$

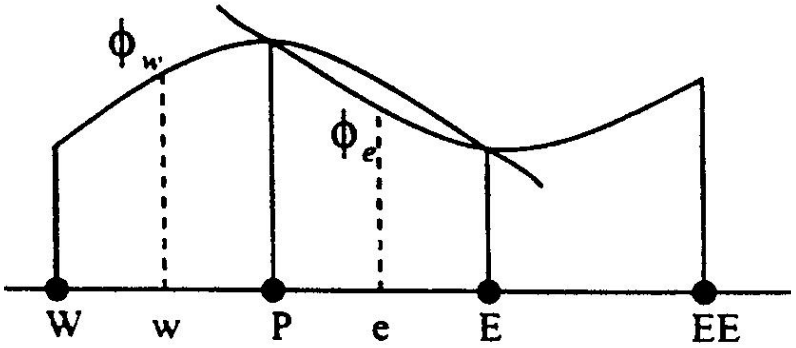

b) $F_e < 0$ and $F_w < 0$

Figure 2: The QUICK scheme.

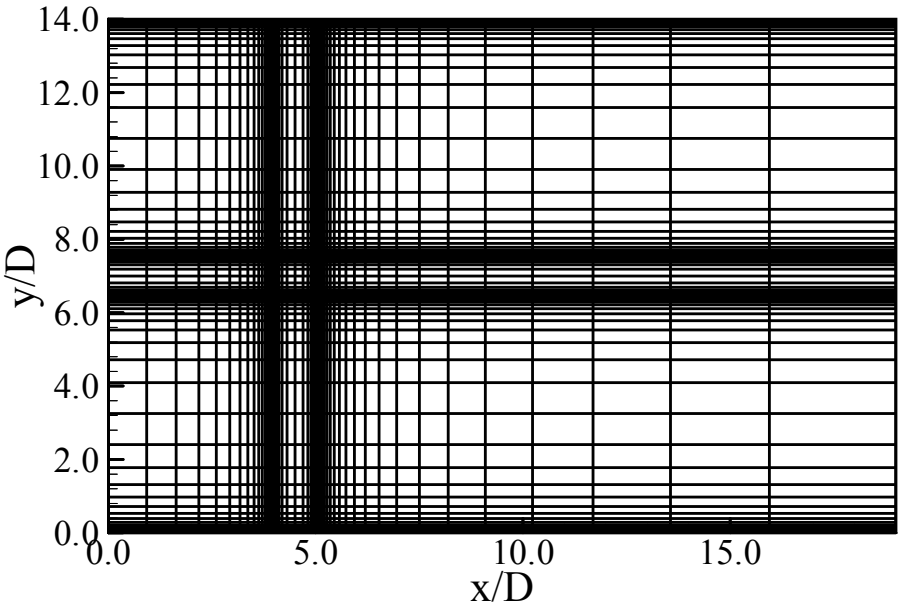

Figure 3: Computational grid with 105×102 grid nodes ($\beta = 7\%$ Re=22000).

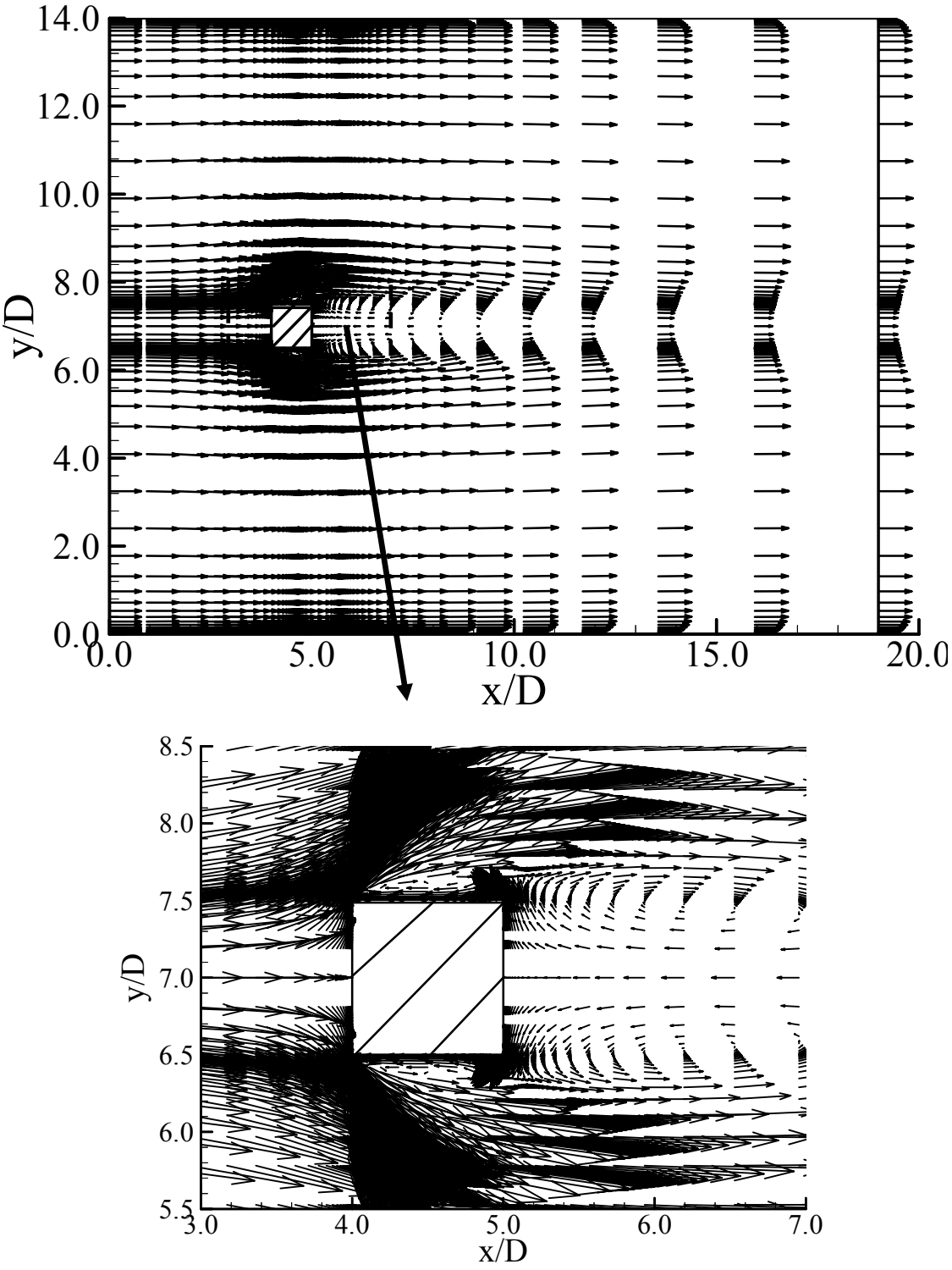

Figure 4: Steady velocity vector around a square cylinder using LS model ($\beta = 7\%$ Re=22000).

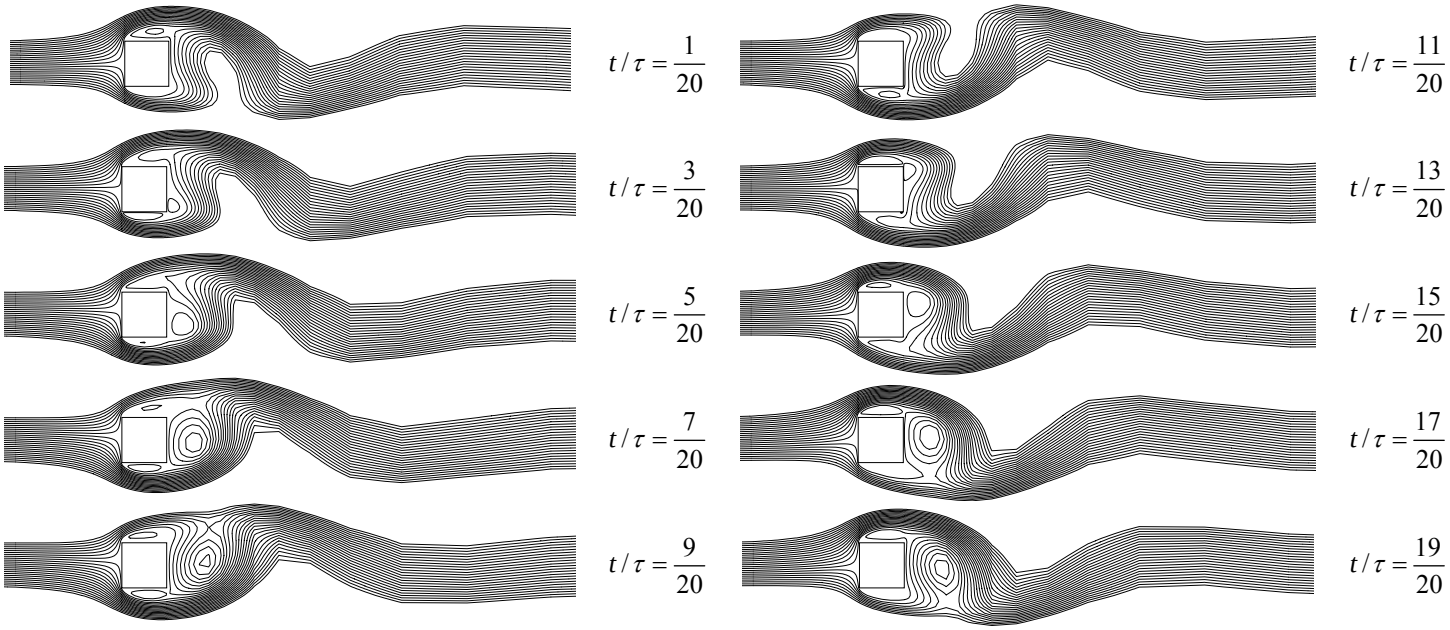

Figure 5: Predicted stream-lines at one period and at 10 different time step using LS model ($\beta = 7\%$ Re=22000).

.

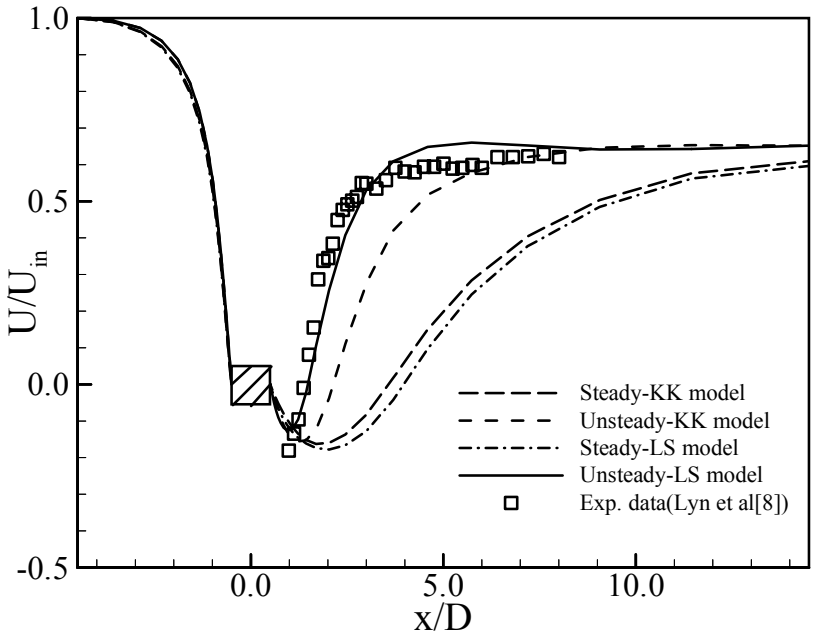

Figure 6: Comparison between stream-wise velocities with experimental data along centerline of the channel.

.

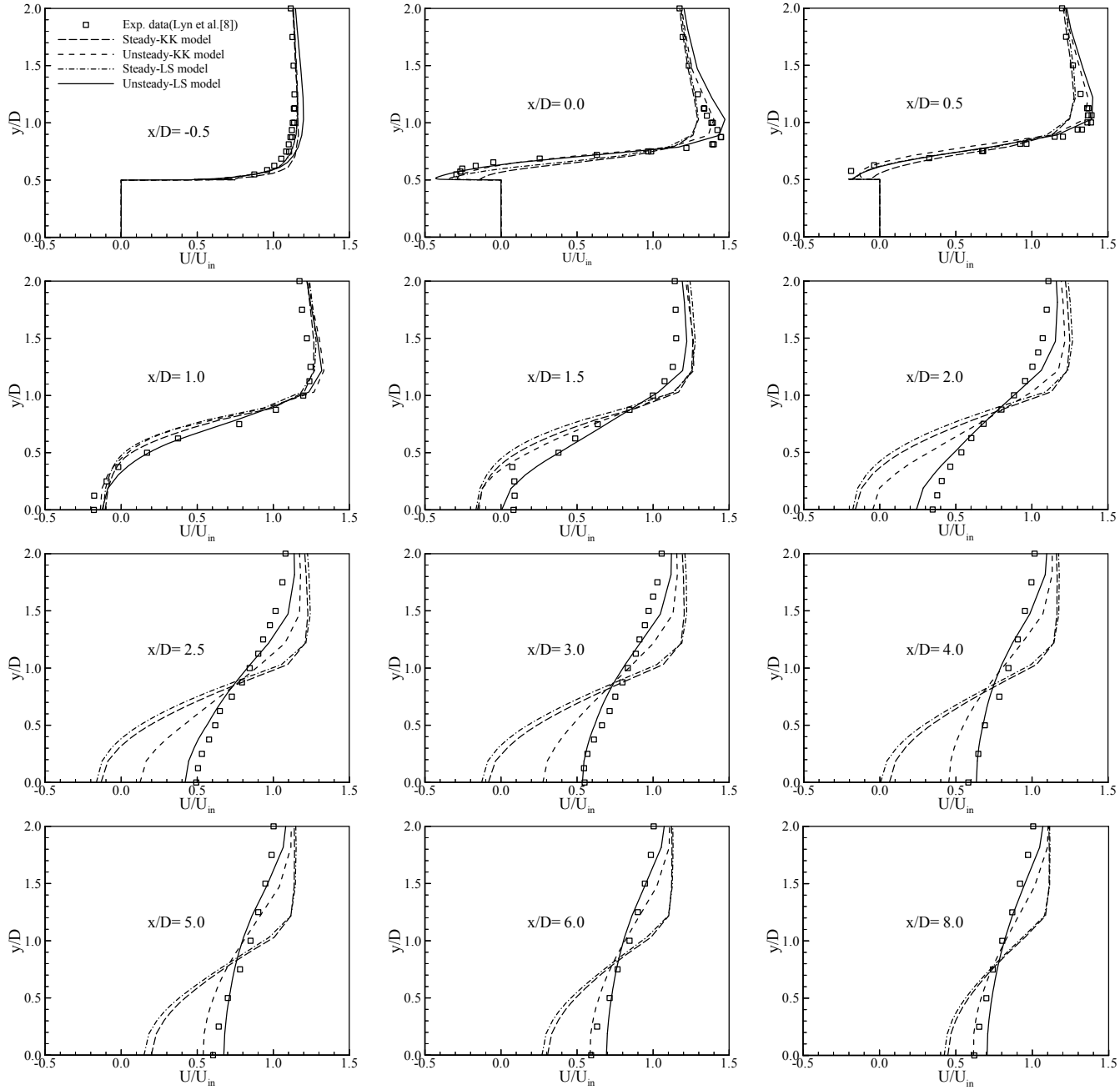

Figure 7: Comparison between predicted stream-wise velocity with experimental data ($\beta = 7\%$ Re=22000).

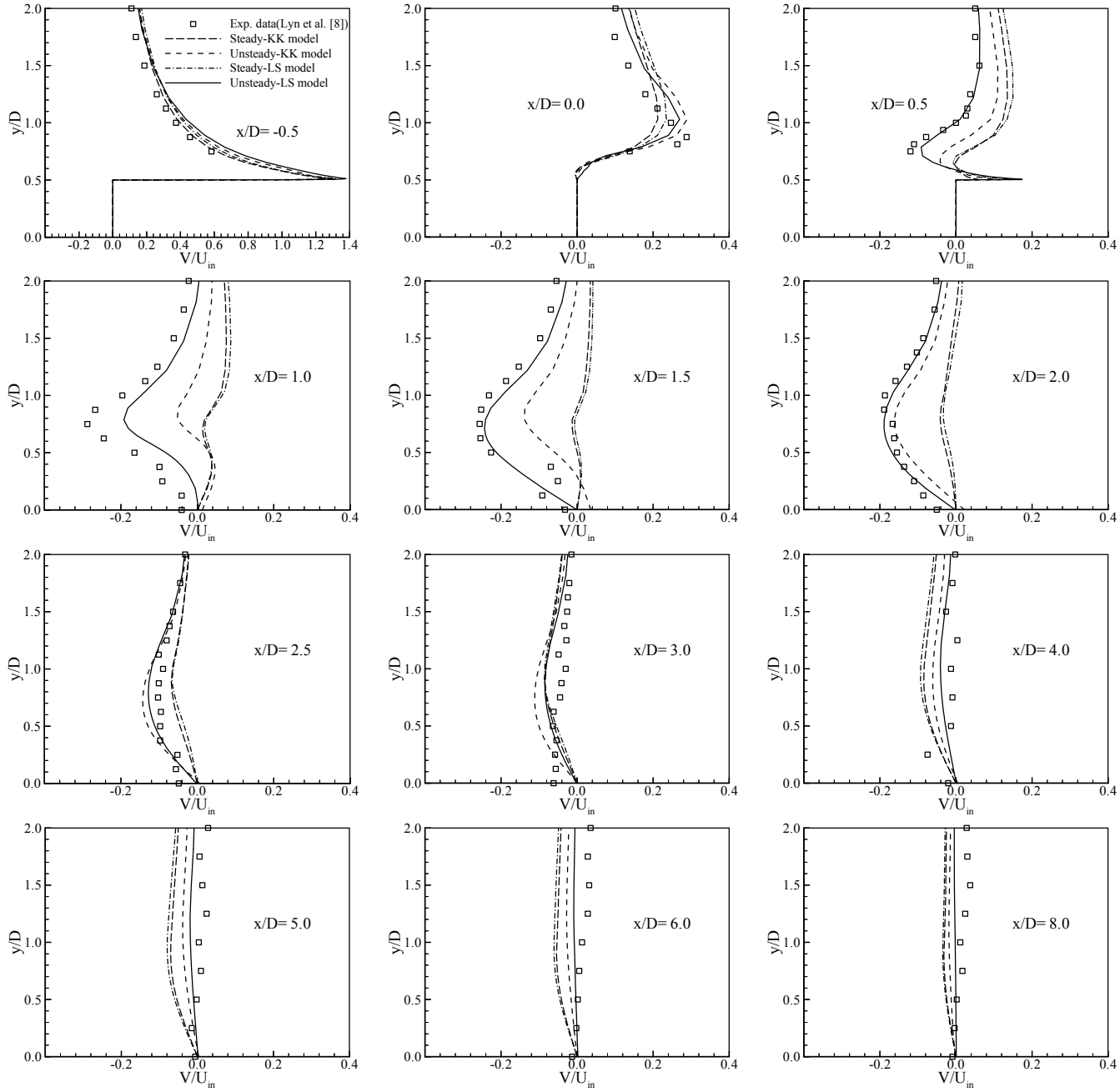

Figure 8: Comparison between predicted cross-stream velocity with experimental data ($\beta = 7\%$ Re=22000).

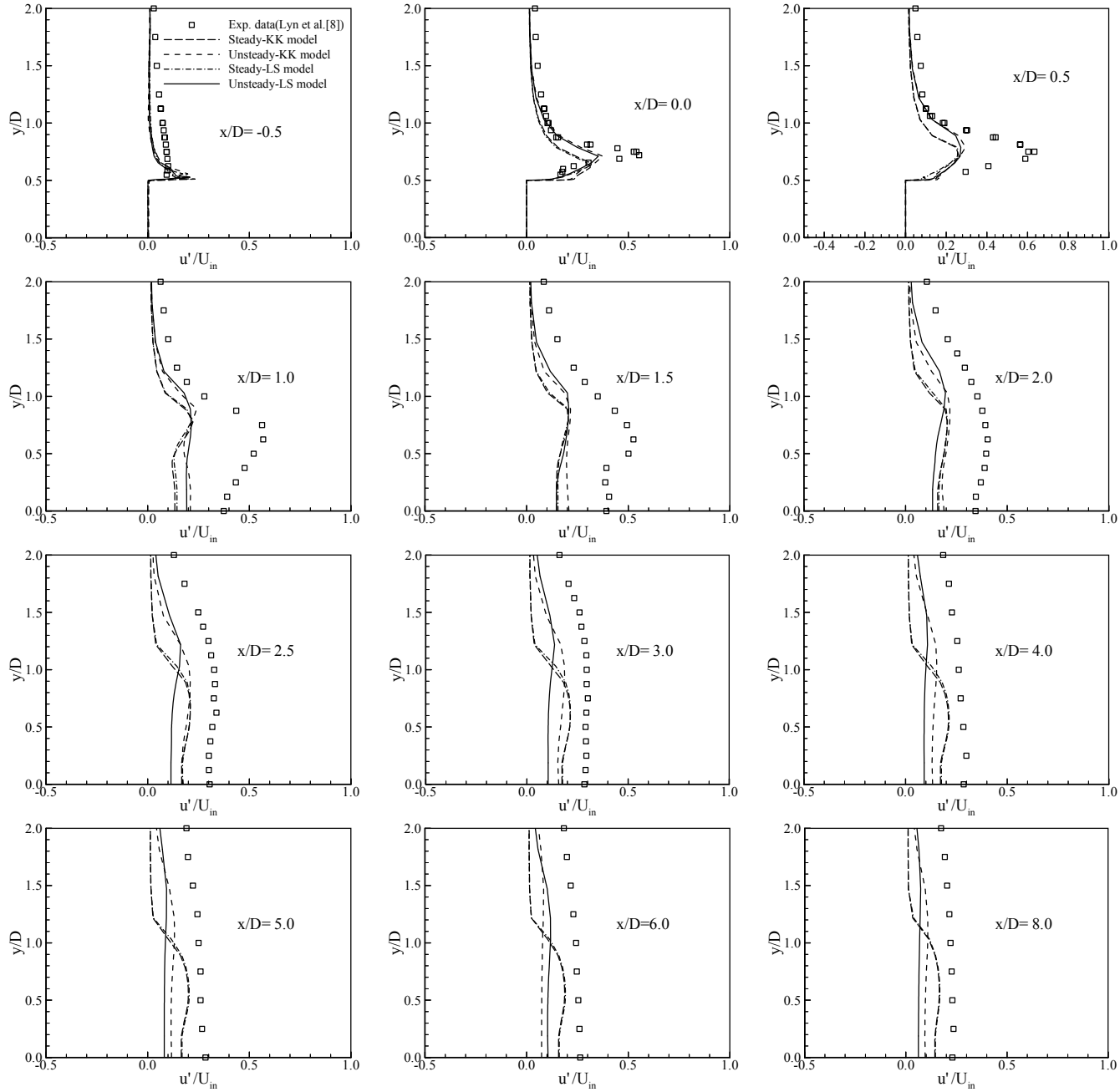

Figure 9: Comparison between predicted stream-wise fluctuation with experimental data (β = 7% Re=22000).

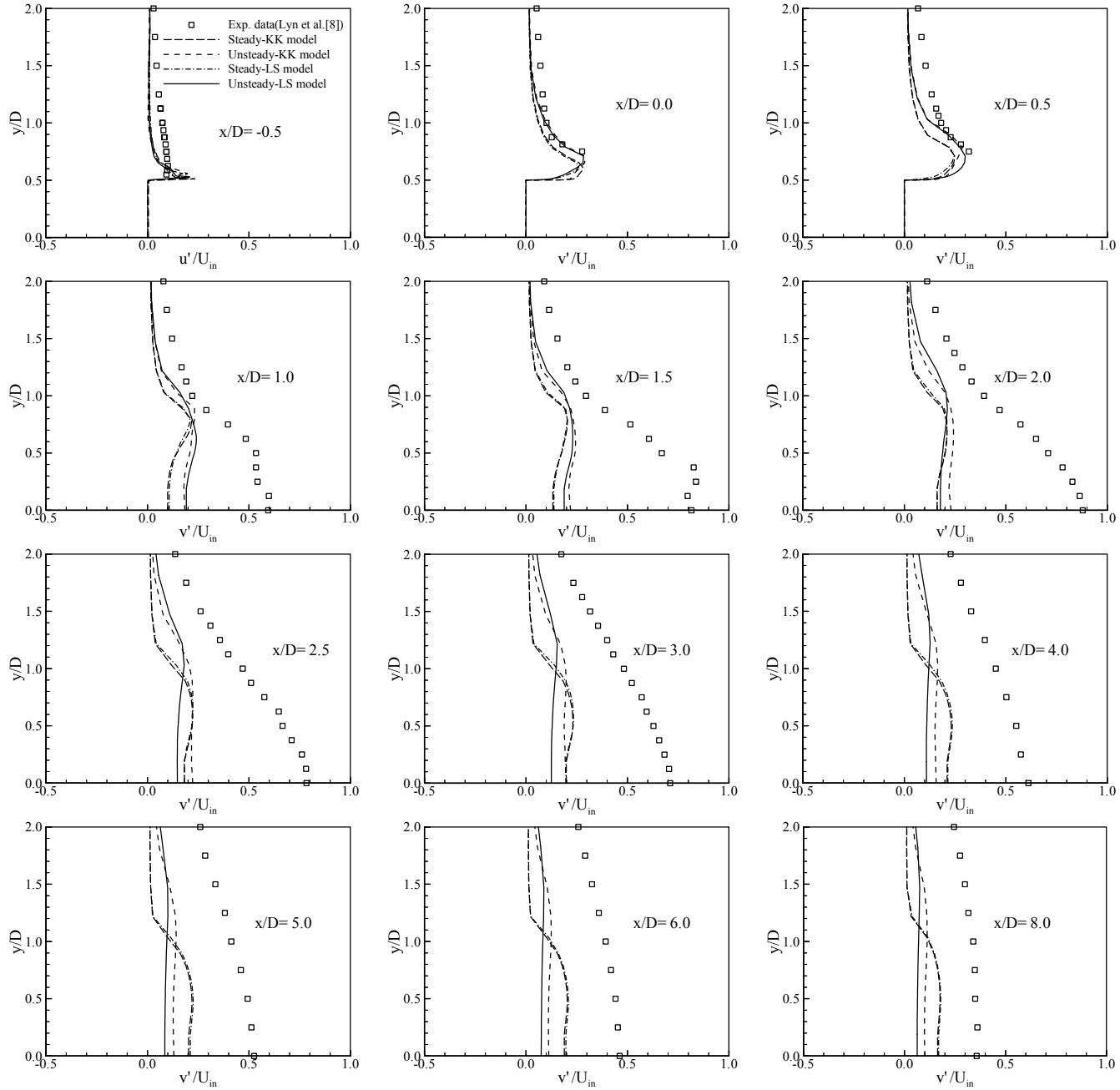

Figure 10: Comparison between the predicted cross-stream fluctuation with experimental data ($\beta = 7\%$ Re=22000).